Biophysical Journal Volume 69 September 1995 1036–1045

Analysis of the Structure of Dimeric DNA Catenanes by Electron Microscopy

Stephen D. Levene,* Clement Donahue,‡ T. Christian Boles,‡ and Nicholas R. Cozzarelli‡

Program in Molecular and Cell Biology,* University of Texas at Dallas, Richardson, Texas 75083; and ‡Department of Molecular and Cell Biology, University of California, Berkeley, Berkeley, California 94720 USA

ABSTRACT We analyzed the structure of open-circular and supercoiled dimeric DNA catenanes generated by site-specific recombination in vitro. Electron microscopy of open-circular catenanes shows that the number of duplex crossings in a plane is a linear function of the number of catenane interlinks (*Ca*/2), and that the length of the catenane axis is constant, independent of *Ca*. These relationships are similar to those observed with supercoiled DNA. Statistical analyses reveal, however, that the conformations of the individual rings of the catenanes are similar to those of unlinked circles. The distribution of distances between randomly chosen points on separate rings depends strongly on *Ca* and is consistent with a sharp decrease in the center-of-mass separation between rings with increasing *Ca*. Singly linked supercoiled catenanes are seen by microscopy to be linked predominantly through terminal loops in the respective superhelices. The observations suggest that chain entropy is a major factor determining the conformation of DNA catenanes.

INTRODUCTION

Supercoiling, knotting, and catenation are three common higher-order structures involving coiling of the DNA axis. DNA catenanes, the subject of this report, are DNA rings that are linked one or more times. They are formed in different biological processes. Catenanes are the products of DNA replication and recombination involving circular genomes and are the substrate for topoisomerases (Sundin and Varshavsky, 1981; Bliska and Cozzarelli, 1987; Ullsperger et al., 1995). The kinetoplast DNA found in the mitochondria of a number of unicellular parasites, such as *Leishmania* and *Crithidia*, consists of large, stable networks of catenated DNA rings (Simpson, 1987; Ryan et al., 1988). Despite the importance of catenated DNA, little is known about its structure in solution. We have analyzed the structure of dimeric DNA catenanes by electron microscopy, to examine geometric features of these forms.

We restricted ourselves to the topological family of structures called torus catenanes (Fig. 1). These are so called because they can be drawn without intersection on the surface of a torus. This is a topological definition, not a geometric one. No deformation, short of breakage and reunion of the DNA phosphodiester backbone, can change a torus catenane into any other form. Torus catenanes are intermediates in DNA replication (Sundin and Varshavsky, 1981; Adams et al., 1992) and products of site-specific recombination systems such as bacteriophage λ integrative recombination and Tn3 resolvase (Mizuuchi et al., 1980; Spengler et al., 1985; Wasserman and Cozzarelli, 1986; Bliska and Cozzarelli, 1987). Recombination by the λ integrative system also provides a convenient method to synthesize catenanes for structural and biochemical studies. It generates molecules in which the winding of the rings around each other is right-handed. Torus catenanes are characterized by the value of a topological invariant, the minimal number of duplex crossings in a projection of the catenane. We denote this quantity *Ca*, and it is twice the linking number between the catenane rings.

Torus catenanes are frequently depicted in one of the two topologically equivalent but geometrically distinct forms shown in Fig. 1. In the form shown in Fig. 1 *A*, the two rings are wound uniformly around a common toroidal axis and share a common center of mass. The form shown in Fig. 1 *A* is an example of a class of structures in which the curvature of DNA, and hence the DNA elastic energy, can be minimized. The reduction of elastic energy in these forms occurs at the expense of catenane entropy, however, as the rings are constrained by their mutual regular geometry. The second form, shown in Fig. 1 *B*, represents a class of structures with higher elastic energy because the windings are concentrated in a limited region of overlap between the rings. The greater conformational freedom of molecules in this class suggests that these structures are expected to be entropically more favorable. One objective of our study was to determine whether the average structure of dimeric catenanes is well described in terms of a particular geometric model. This approach has previously been successful in deriving the average geometry of extensively supercoiled DNA (Boles et al., 1990).

The constraint of right-handed winding of the DNA duplexes in Int catenanes imposes a geometry on each ring, which can be inferred from the change in the DNA linking number, *Lk*, after nicking and religation of the DNA (Was-

Received for publication 1 December 1994 and in final form 15 June 1995.

Address reprint requests to Dr. Nicholas R. Cozzarelli, Department of Molecular and Cellular Biology, University of California, Berkeley, 401 Barker Hall, Berkeley, CA 94720-0001. Tel.: 510-542-5266; Fax: 510-542-7000; E-mail: cozzlab@garnet.berkeley.edu.

Dr. Donahue's present address is Department of Pediatrics, University of California Medical Center, San Francisco, CA 94143-0110.

Dr. Boles' present address is Mosaic Technologies, 800 Huntington Avenue, Boston, MA 02115.

0006-3495/95/09/1036/10 $2.00

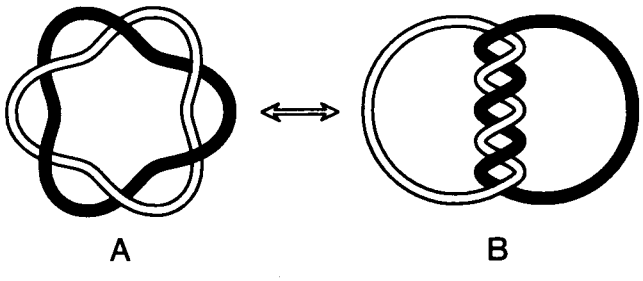

FIGURE 1 Idealized models of a torus catenane. Individual rings of a catenane are indicated by the filled and open curves. The two forms are topologically equivalent, indicated by the double-headed arrow. (*A*) Toroidal catenane geometry, in which the catenane rings are wrapped around the surface of a virtual torus. (*B*) Locally interwound catenane geometry, in which the catenane links are concentrated in a region of overlap between the two rings.

serman et al., 1988). The result is that the change in *Lk* is proportional to *Ca*. Monte Carlo simulations show that this change in *Lk* is mostly a result of positive writhe, *Wr*, induced by the mutual intertwining (Vologodskii and Cozzarelli, 1993). A linear dependence of *Wr* on ΔLk is also a property of supercoiled DNA deduced by electron microscopy (Boles et al., 1990) and Monte Carlo simulations (Vologodskii et al., 1992).

We examined the conformation of open-circular, multiply linked dimeric catenanes by electron microscopy. The catenanes were prepared by Int recombination of supercoiled DNA substrates, which were converted to open-circular form by DNase I nicking to remove the contributions of supercoiling to conformational properties. Catenanes with specific values of *Ca* were resolved by gel electrophoresis and isolated for further study. The catenated Int products contain rings nearly identical in length; this information in conjunction with the minimal number of catenane crossings expected from the value of *Ca* allowed the structure of individual catenanes to be determined.

We find that over the relatively low range of *Ca* studied ($6 \leq Ca \leq 18$), nicked torus catenanes do not have a regular geometry but instead are best described as irregular structures in which the ring centers of mass are significantly separated. Increasing *Ca* does strongly decrease the center-of-mass separation. The results show that the structure of catenane rings is similar to that of a cyclic random coil and is not strongly dependent on the *Ca* value. Despite the irregularities in the structure of individual catenanes, some catenane properties behave systematically over this *Ca* range. We find that the average length of the axis defined by the winding of the two duplex DNAs is constant and that the number of crossings of the two duplex chains in the micrographs is a little more than *Ca*.

We also analyzed the structure of singly linked, supercoiled catenanes prepared by Tn3 resolvase site-specific recombination (Wasserman and Cozzarelli, 1986). We found that the single interlink occurs predominantly near the terminal loop of a superhelix; 83% of the molecules were linked through at least one end, and 40% were linked through both terminal loops.

Although the structures of individual catenanes do not closely resemble either of the structures shown in Fig. 1, the overall behavior of our measured parameters as a function of *Ca* suggests that chain entropy is an important factor in the structure and organization of catenanes. Our study is intended to provide a semiquantitative picture for interpreting the properties of catenated DNA in terms of general physical principles.

MATERIALS AND METHODS

Plasmid DNA

pAB7.0d is a 7 kb plasmid containing *attP* and *attB* sites for Int recombination in direct orientation and also *res* sites for Tn3 resolvase recombination (Wasserman et al., 1988; Benjamin and Cozzarelli, 1990). pJB3.5d is a 3.5 kb plasmid with *att* sites in direct orientation (Bliska and Cozzarelli, 1987) and served as a control in experiments requiring nicked, unlinked circles. DNA was prepared by using the alkaline lysis method (Sambrook et al., 1989) and purified twice by CsCl-ethidium bromide density-gradient centrifugation. Ethidium bromide was removed by a series of extractions with butanol, and the plasmid was dialyzed against Tris-EDTA (TE) buffer (10 mM Tris-Cl, pH 8.0, 1 mM Na_2EDTA). The DNA was precipitated with isopropanol, resuspended at a concentration of ~1 mg/ml in TE buffer, and stored at 4°C.

Enzymatic reactions

Tn3 resolvase (Krasnow and Cozzarelli, 1983), *E. coli* integration host factor (IHF) (Nash and Robertson, 1981; Nash et al., 1987), and wheat germ topoisomerase I (Dynan et al., 1981) were prepared as described. Int protein was a generous gift of H. Echols, University of California, Berkeley. DNase I and restriction enzymes were obtained commercially.

Int reactions were carried out in either a standard buffer (20 mM Tris-Cl, pH 7.6, 50 mM NaCl, 20 mM KCl, 10 mM $MgCl_2$, and 50 μg/ml bovine serum albumin) to generate distributions of complex catenane products, or modified buffer conditions (50 mM Tris-Cl, pH 7.6, 20 mM KCl, 5 mM spermidine, 2 mM Na_2EDTA, and 2 mg/ml albumin) to increase the yield of low *Ca* products. Reaction mixtures contained 2.5 μg Int, 35 ng IHF, and 2.5 μg DNA in 25 μl and were incubated at 25°C for 30 min. Reactions were stopped by heating to 65°C for 5 min.

Resolvase reactions contained 10 mM Tris-Cl, pH 7.5, 150 mM NaCl, 10 mM $MgCl_2$, 1.5 μg resolvase, and 2 μg DNA in a volume of 40 μl. Incubations were at 37°C for 30 min, and the reaction was terminated by heating to 65°C for 5 min.

Open-circular catenanes were prepared by limited nicking with DNase I (0.5 μg/ml) in the presence of 0.3 mg/ml ethidium bromide (Barzilai, 1973). Reactions lacking $MgCl_2$ were supplemented to a final concentration of 10 mM Mg^{2+} before addition of DNase I. After 30 min at 37°C, the mixtures were heated to 65°C for 5 min, extracted three times with phenol-chloroform (1:1) and once with chloroform, and precipitated with isopropanol.

Partially relaxed DNA substrates were obtained by treatment of natively supercoiled plasmid DNA with wheat germ topoisomerase I in the presence of ethidium bromide. Reaction mixtures contained 0.5–10 μg/ml ethidium bromide, 25 units topoisomerase I, and 25 μg DNA in 50 μl total volume of standard or modified Int buffer. After 1 h at 37°C, reactions were stopped by adding sodium dodecyl sulfate (SDS) to 0.1% and extracted three times with phenol-chloroform, once with chloroform, and five times with TE-saturated butanol. The DNA was precipitated with ethanol and resuspended in TE buffer.

Gel electrophoresis

Mixtures of catenanes obtained by Int recombination were separated by high-resolution gel electrophoresis using 0.8% agarose gels. Electrophoresis was in TAE buffer (80 mM Tris-acetate, pH 7.9, 5 mM sodium acetate, 1 mM Na_2EDTA) containing 0.03% SDS (Sundin and Varshavsky, 1981) for 18–30 h using an applied field of 1.2 V/cm. To visualize the DNA, gels were soaked in TAE buffer (lacking SDS) for 1–2 h, stained in 0.5 μg/ml ethidium bromide for 30 min, and destained for 1–2 h in TAE buffer before viewing and photography using an ultraviolet transilluminator.

Preparation of purified catenanes

Individual catenane species were purified by excising a specific band from a high-resolution gel and extracting the DNA using a freeze-thaw technique. The gel slice was pulverized by forcing it through a syringe, vortexed vigorously with ⅓ volume phenol for 60 s, and frozen in liquid nitrogen. The phenol-agarose slurry was thawed to room temperature and spun in a tabletop centrifuge at 3400 rpm for 10 min. The aqueous supernatant was removed, and the phenol-agarose slurry was vortexed with 1/24 volume TE buffer for 60 s and once again frozen in liquid nitrogen. Upon thawing, the centrifugation step was repeated and the supernatant pooled with the aqueous layer obtained from the first extraction. The aqueous layer was extracted once with phenol-chloroform (1:1) and once with chloroform, and the DNA precipitated with ethanol.

Electron microscopy

DNA molecules were applied to poly-L-lysine-coated, thin carbon films supported on electron microscope grids (Boles et al., 1990). Samples were rotary shadowcast in a Varian (Palo Alto, CA) evaporator using evaporated tungsten wire under a vacuum of $0.6–1.0 \cdot 10^{-5}$ mm Hg. A shadowing angle of 8° was used. Examination of grids and photography of molecules were done using a JEOL (Peabody, MA) 1200EXII electron microscope. Observations were carried out using accelerating voltages of 40 or 80 kV with a 40 μm objective aperture.

Image analysis

Contours of molecules were projected from micrograph negatives using an enlarger and traced by hand on sheets of paper. Hardcopy tracings of the rings were digitized individually using a digitizing tablet interfaced to an IBM PC-AT running Sigma-Scan software (Jandel Scientific, San Rafael, CA) and were stored on disk for subsequent analysis. Some analyses were done on images captured directly from negatives with an Eikonix (Ektron Applied Imaging (Bedford, MA) 1412 diode array camera interfaced to a VAXStation (Digital Equipment Corp., Woburn, MA) 3100 workstation. The molecular contours in these digitized images were traced using SigmaScan/Image software (Jandel Scientific).

Analysis of distance distributions was carried out on sets of 25–40 catenane tracings using software written by one of the authors (S. D. L.). Plots of catenane tracings were done using SigmaPlot software (Jandel Scientific).

RESULTS

Electron microscopy of open-circular, multiply linked, dimeric DNA catenanes

We generated torus DNA catenanes with a defined topology by site-specific recombination using the Int system of phage λ. The substrate used in these experiments, pAB7.0d, is a 7.0 kb plasmid bearing Int recombination (*att*) sites in direct orientation with a spacing of 3.5 kb (Wasserman et al., 1988; Benjamin and Cozzarelli, 1990). With this equal spacing of the *att* sites, recombination forms catenane products consisting of identically sized pairs of rings. The distribution of *Ca* values in the recombination products is determined by the distribution of the number of supercoils trapped at site synapsis (Benjamin and Cozzarelli, 1986; Bliska and Cozzarelli, 1987; Wasserman et al., 1988), and the average value of *Ca* is a linear function of the linking-number deficit, ΔLk (Boles et al., 1990). Int recombination of natively supercoiled DNA substrates generated products with a broad distribution of *Ca* values ranging from 4 to ~18 (Fig. 2 *A*) (Mizuuchi et al., 1980).

To improve the yield of catenanes with low values of *Ca*, we reduced the superhelix density of the substrates. Partially relaxed substrates were prepared by treating pAB7.0d with topoisomerase I in the presence of ethidium bromide at varying concentrations. The yield of low-*Ca* products was further improved by recombining substrates with low superhelix density under modified Int conditions, in which spermidine replaces Mg^{2+} as the multivalent counterion (Fig. 2 *B*). These conditions are identical to those under which Int recombines nicked DNA (Pollock and Nash, 1983). Nicked catenane products were separated by gel electrophoresis, isolated from the gel, and prepared for electron microscopy.

More than 200 molecules were traced and analyzed from micrographs; examples are shown in Fig. 3. Although the contour of duplex DNA can clearly be seen, the two rings of

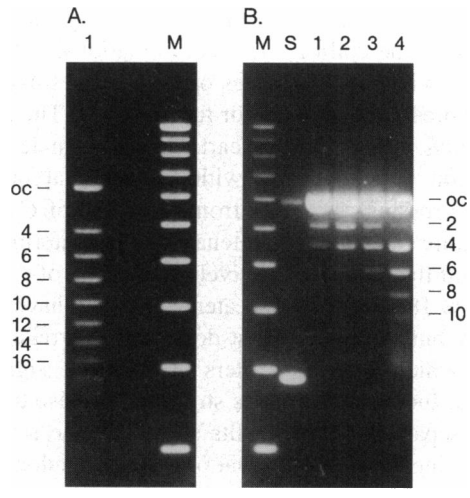

FIGURE 2 Distribution of multiply linked catenane products generated by Int recombination. Plasmid pAB7.0d with varying superhelix densities was incubated with Int in the presence of IHF to generate the mixtures of catenanes shown here. After limited nicking with DNase I, the products were separated by electrophoresis for 21 h in a 0.8% agarose gel at 1.2 V/cm. Lanes labeled *M* contain a 1 kb marker ladder; lane *S* contains the untreated supercoiled substrate. (*A*) Products of recombination generated by using natively supercoiled substrates. (*B*) Recombination of partially relaxed substrates. Lanes 1–4 contain Int recombination products of substrates relaxed in the presence of 1, 2, 4, and 8 μg/ml ethidium bromide, respectively. The bands corresponding to the recombination products are indicated by the values of *Ca* on the left and on the right; *oc* indicates the position of the nicked-circular substrate.

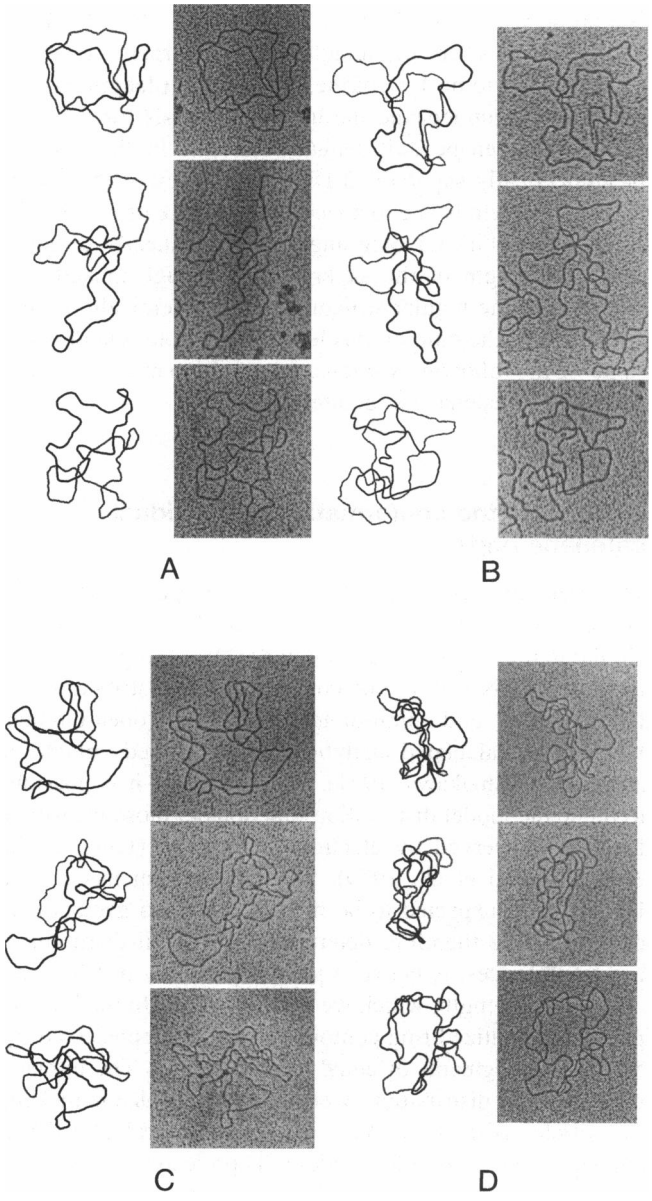

FIGURE 3 Electron micrographs and corresponding tracings of multiply linked catenane rings. Dimeric catenanes were prepared by Int recombination of plasmid pAB7.0d, generating multiply linked rings, each 3.5 kb in size. Catenane DNA samples with known values of *Ca* were purified by gel electrophoresis and applied to carbon-coated electron-microscope grids. The DNA contour was traced from a projection of the negative, and catenane rings were identified by locating two closed paths of monomer contour length that generated a number of duplex crossings equal to or greater than the value of *Ca*. Three examples of each of four values of *Ca* are shown: (*A*) $Ca = 6$, (*B*) $Ca = 10$, (*C*) $Ca = 14$, (*D*) $Ca = 18$.

the catenane are frequently highly entangled, particularly at high values of *Ca*. Despite this, the connectivity of DNA segments in these two-dimensional (2D) images could be established because of two additional pieces of information. First, because the catenanes were purified by gel electrophoresis, the *Ca* value and hence the number of duplex crossings in a minimal projection of each catenane was known. Second, the contour lengths of each ring were known from the contour separation of the recombination sites. Catenane tracings from electron micrographs were analyzed by following the DNA along a closed path whose length is within 10% of the known contour length. The projected contour length of the second duplex ring was then measured and compared with the known value. Structures that satisfied these contour length criteria and also had numbers of inter-ring crossings greater than or equal to *Ca* were digitized and the 2D coordinates of each ring stored on disk. Between 15 and 30 catenanes were analyzed for each value of *Ca*.

Fig. 3 shows examples of isolated catenanes with $6 \leq Ca \leq 18$ and the corresponding tracings of individual rings identified using the procedure described above. Despite the fact that these molecules have net positive *Wr*, there is a high degree of variability in the conformations of the catenanes. In many cases, the catenane rings do not overlap strongly, but share only a limited region of intertwining.

Numbers of duplex crossings in multiply linked catenanes

Fig. 4 shows as a function of *Ca* both the average total number of duplex crossings and the average number of crossings occurring between the two catenane rings (interannular crossings). Both the average total number of crossings and the average number of interannular crossings show a linear variation with unit slope over the range of *Ca* values studied ($6 \leq Ca \leq 18$). The average number of interannular duplex crossings is only slightly greater than the value of *Ca* (Fig. 4). Therefore, most of the crossings in excess of the *Ca* value arise from crossings of one of the rings with itself and

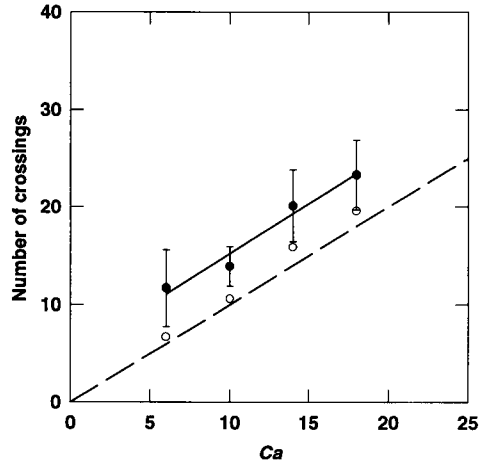

FIGURE 4 Number of interannular crossings as a function of *Ca*. Tracings of catenanes were used to determine the number of crossings within and between the rings. The average number of crossings for 15–30 structures for each *Ca* value is shown. (●) Average number of total crossings. (○) Average number of interannular crossings. A dashed line indicates the minimal number of interannular crossings. Error bars indicate one standard deviation.

there is very little accidental overlay of the two rings. This results in part from the separation of the linked rings noted above. The number of excess crossings is independent of *Ca* within error and equal to 5.0 ± 0.3. This observation is consistent with a model in which the structure of individual rings is not strongly dependent on the *Ca* value.

Dimensions of the catenane axis

As with supercoiled DNA, we define the axis of the catenane to be the curve that passes through chain crossings (nodes) and the midpoints of line segments connecting pairs of opposing points on each catenane ring. Because of the irregular structure of nicked catenanes we adopted several rules to improve consistency in tracing the catenane axis through loops in the structures. First, we assigned the same orientation to both duplexes and imposed the condition that the axis also have this orientation. Second, "bulges" or instances in which one ring looped away from the other without crossing itself were treated such that the axis continued to follow from the midpoint of line segments that connect opposing points. Third, "flops" or situations in which one ring looped away from the other while crossing itself were accommodated by permitting breaks in the axis in order to be consistent with the parallel orientation rule. With these rules, the catenane axis was traced for each micrograph analyzed, and the average lengths are plotted in Fig. 5 as a function of *Ca*.

Within error, the average length of the catenane axis is independent of *Ca* over the range studied here and equal to 975 nm, 41% of the total DNA contour length (2380 nm). The constancy of axis length with increasing DNA winding is a property previously shown for supercoiled DNA (Boles et al., 1990), where the length of the superhelix axis was also observed to be 41% of the DNA contour length. We do not presently understand the underlying basis for the constancy of catenane axis length with *Ca*. In the case of plectonemically supercoiled DNA, constancy of the superhelix axis length is due to a weak dependence of axis length on the superhelix winding angle, which is nearly constant along the length of the superhelix. Although nicked catenanes lack the regular structure of plectonemically supercoiled DNA, the ratio of axis length to contour length is the same. In the following sections, we turned to more objective measures of catenane structure.

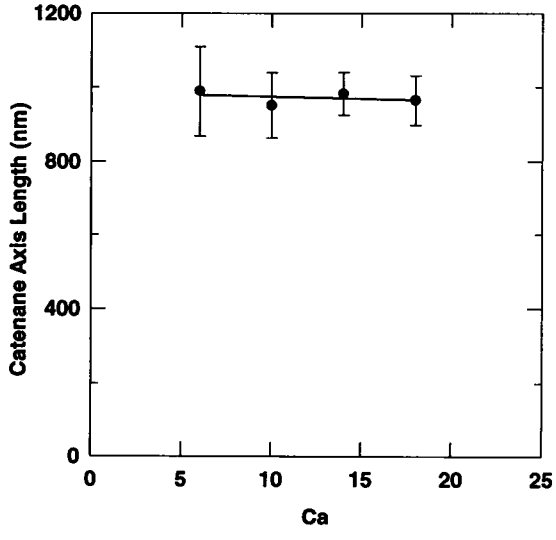

FIGURE 5 Length of the catenane axis as a function of *Ca*. Tracings of catenanes were used to determine the length of the catenane axis, defined as a curve that passes midway through line segments that connect corresponding pairs of points on the catenane rings. The line is the least-squares linear fit to the axis-length data with slope equal to −1.0 and an intercept equal to 984. Error bars indicate one standard deviation.

Analysis of the conformation of individual catenane rings

The irregular appearance of the rings in open-circular catenanes suggests that the dimensions of these rings may be similar to those of free, open-circular DNA. Simple polymer models for DNA allow the conformational distributions of intermediate- and high-molecular-weight, open-circular DNA to be calculated analytically, if excluded volume is neglected (Yamakawa, 1971). In some cases, it is possible to relate the model distribution functions to those measured for DNA observed by electron microscopy (Lang et al., 1967; Frontali et al., 1979). The longest dimension of a DNA ring is expected to be most sensitive to geometrical distortion. We therefore determined the radial distribution of pair distances, ρ, between points spaced by one-half the ring contour length, which we denote $P_{tra}(\rho)$. In these computations, digitized ring contours were each represented by 50 discrete segments of equal contour length. The intraannular distance distributions were compared to that in nicked, free circles ($Ca = 0$). As a reference, we calculated the analytical distribution for random 2D projections of a three-dimensional (3D) cyclic random coil. The expression for this distribution is given in the Appendix.

Fig. 6 shows $P_{tra}(\rho)$ plotted for *Ca* equal to 0, 6, 10, 14, and 18, along with the cyclic random coil control. The distributions are nearly independent of *Ca* except for some truncation of the tail of the distribution at large separations in the highest complexity catenane analyzed ($Ca = 18$). The differences between this distribution and those at lower catenane complexity ($0 \leq Ca \leq 14$) are, however, not far outside of the noise level of the data.

The truncation of the distribution for higher complexity catenanes can be rationalized as follows. Extended conformations of catenanes with more highly intertwined rings are presumably less probable, because the formation of an extended conformation in one ring also requires extension of the second ring when the rings are tightly intertwined. The lack of *Ca* dependence of the distribution for short distances indicates that catenation does not greatly affect the tendency of a ring to loop back on itself for relatively low values of *Ca*. The most probable loop size in DNA is in the neigh-

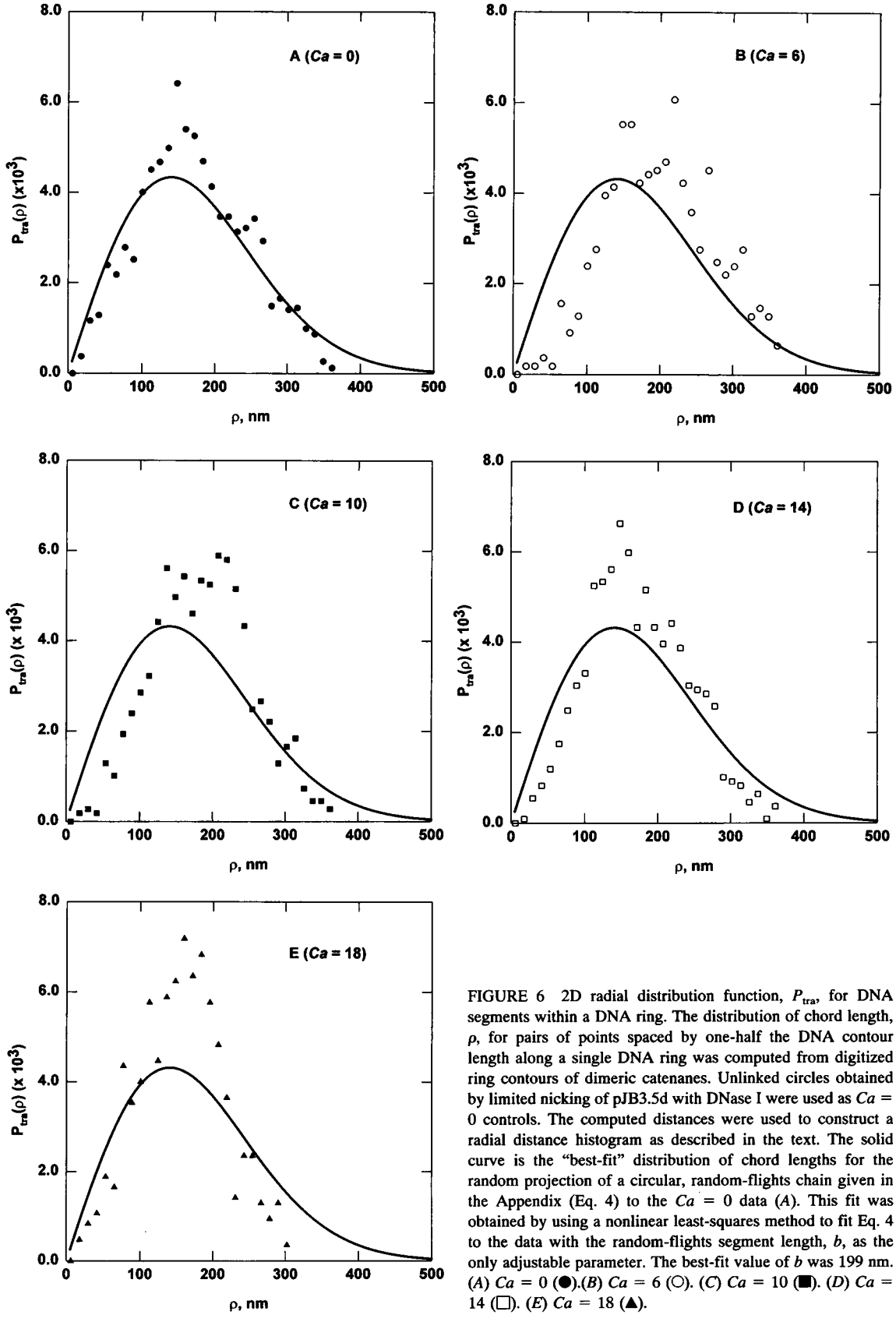

FIGURE 6 2D radial distribution function, P_{tra}, for DNA segments within a DNA ring. The distribution of chord length, ρ, for pairs of points spaced by one-half the DNA contour length along a single DNA ring was computed from digitized ring contours of dimeric catenanes. Unlinked circles obtained by limited nicking of pJB3.5d with DNase I were used as Ca = 0 controls. The computed distances were used to construct a radial distance histogram as described in the text. The solid curve is the "best-fit" distribution of chord lengths for the random projection of a circular, random-flights chain given in the Appendix (Eq. 4) to the Ca = 0 data (*A*). This fit was obtained by using a nonlinear least-squares method to fit Eq. 4 to the data with the random-flights segment length, b, as the only adjustable parameter. The best-fit value of b was 199 nm. (*A*) Ca = 0 (●).(*B*) Ca = 6 (○). (*C*) Ca = 10 (■). (*D*) Ca = 14 (□). (*E*) Ca = 18 (▲).

borhood of 500 bp (Shore and Baldwin, 1983). Catenation is therefore not expected to affect the formation of relatively short loops unless the average distance between interlinks along a single ring is significantly shorter than the average loop size.

The distribution of distances between rings

Although catenation has only small effects on the distribution of distances between pairs of points on a single ring, catenation should have a strong effect on the separation of DNA between rings. This distance, on average, should decrease sharply with increasing catenane complexity, eventually approaching a limiting value that reflects excluded volume effects.

We determined the distributions of distances between randomly chosen pairs of points on separate catenane rings, each ring contour being represented as 50 segments of equal contour length. This distance-distribution function, which we denote $P_{ter}(\rho)$, is shown in Fig. 7 for four values of *Ca*, equal to 6, 10, 14, and 18. We conclude that increased catenane complexity narrows the pair-distance distribution and shifts the maxima to progressively smaller values. Thus, although the intraannular distance distribution of catenane rings is close to that expected for a random coil and is not strongly dependent on catenane complexity, the distribution of interannular pair distances depends markedly on *Ca*.

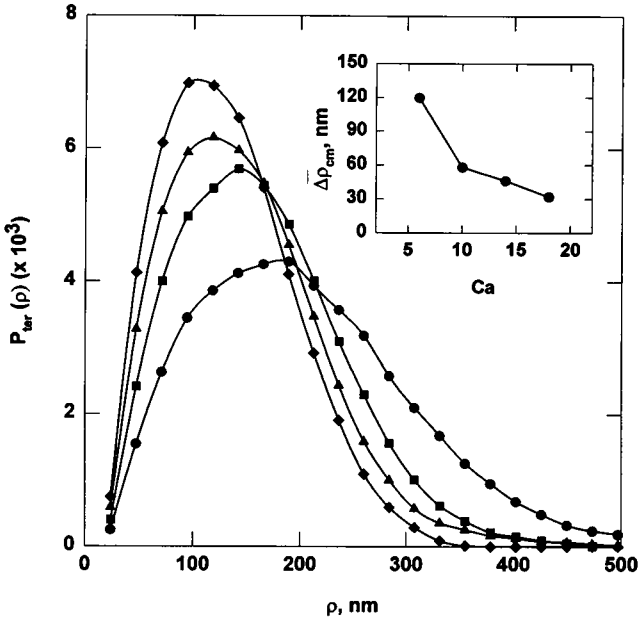

FIGURE 7 Probability distribution function, $P_{ter}(\rho)$, for distances between DNA segments located on separate rings, ρ. Through-space distances between DNA segments located on individual catenane rings were determined for all pairwise combinations of segments from the digitized ring contours and used to construct a distance histogram as in Fig. 6. The average center-of-mass separation of the two rings, $\Delta\bar{\rho}_{cm}$, shown in the inset, was computed from the distance histograms and also independently from the sets of catenane conformations. (●) *Ca* = 6. (■) *Ca* = 10. (▲) *Ca* = 14. (♦) *Ca* = 18.

The tendency of the catenane rings to approach one another with increasing *Ca* is also reflected in the average distance between ring centers of mass, which we determined separately from the sets of conformations. The *Ca* dependence of the ring center-of-mass separation is shown in Fig. 7 (*inset*). There is an initial sharp decrease in average separation between *Ca* = 6 and *Ca* = 10, followed by a more gradual decrease out to *Ca* = 18, the upper limit of our study.

Conformations of supercoiled, singly linked catenanes

Supercoiled, as opposed to nicked-circular catenanes, are frequently the forms that are biologically active and are the most common form found in vivo. Studies of natively supercoiled, multiply linked catenanes using the methods described here foundered, however, because of the large number of DNA overlaps observed (C. Donahue and N. R. Cozzarelli, unpublished results). In the first step toward characterization of the structure of supercoiled catenanes as a function of *Ca*, we analyzed the conformations of singly linked supercoiled catenanes. These were prepared by site-specific recombination with Tn3 resolvase.

Electron micrographs of singly linked supercoiled catenanes are shown in Fig. 8. These molecules closely resemble supercoiled DNA in that they are elongated, branched, plectonemically wound structures. The contour of each ring was determined by identifying the tracing of the catenane that yielded two rings with projected contour lengths within 10% of the known values. Of 37 catenanes analyzed, 92% of the molecules had a single interannular crossing. Thus as with the nicked catenanes, the average number of intermolecular nodes nearly equals *Ca*.

We determined the position along the superhelix axis of the single catenane interlink. In Fig. 9, we plot the joint location of the single interlink along the superhelix axis of each ring relative to the length of the respective axis. A striking result emerges; in 86% of the molecules at least one of the rings is linked through the ends of the plectonemic superhelix, and 40% of the singly linked supercoiled catenanes contained two molecules that were linked through terminal loops of the respective superhelices. The observation that intermolecular linkage in supercoiled catenanes occurs predominantly through terminal loops in the superhelix suggests that these conformations are favorable because of their higher configurational entropy and lower electrostatic free energy.

DISCUSSION

We used electron microscopy to study the structure of open-circular, multiply linked DNA catenanes and also supercoiled, singly linked catenanes. Although sample preparation surely introduces distortions, several considerations justify the use of electron microscopy to estimate the con-

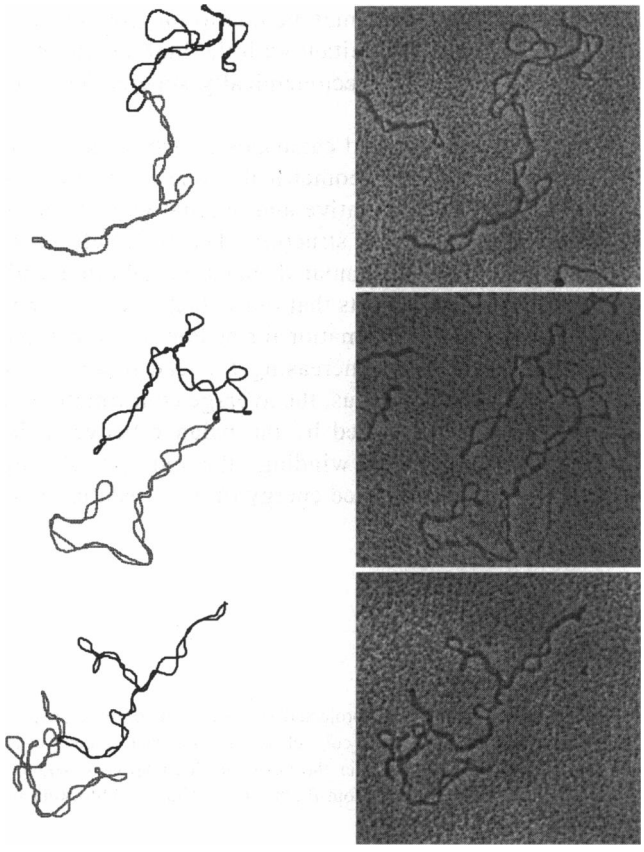

FIGURE 8 Electron micrographs and corresponding tracings of contours of supercoiled, singly linked catenanes. Singly linked catenanes prepared by Tn3 resolvase recombination of pAB7.0d were isolated and prepared for electron microscopy as described in the legend to Fig. 3.

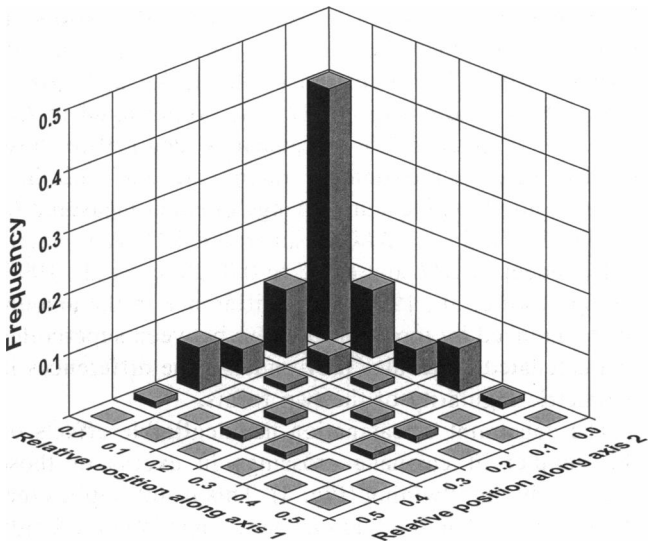

FIGURE 9 Distribution of locations of the single catenane interlink in supercoiled, singly linked catenanes. The location of the interlink along the superhelix axis of each ring was determined relative to the nearest end of the superhelix. The superhelix axis was determined by the same method used previously (Boles et al., 1990). The joint location of the interlink for each pair of rings was then used to construct the 2D frequency plot shown here.

formation of catenated DNA. First, this approach has previously been successful in analyzing the structure of plectonemically supercoiled DNA (Boles et al., 1990). For superhelical DNA, a number of average quantities determined by electron microscopy, including the length of the superhelix axis, the number of superhelical turns, and the ratio of Wr to ΔLk, agree very well with the values of these quantities computed using Monte Carlo simulations (Vologodskii et al., 1992). Second, the data are self-consistent. Intraannular distance distributions over the range of Ca values in the present study are similar to that for uncatenated free circles, and both are similar to that expected for 2D projections of cyclic random coils. Third, there is strong qualitative agreement with the Monte Carlo simulations of catenanes by Vologodskii and Cozzarelli (1993), which do not share any of the assumptions of the present analysis.

Electron micrographs of multiply linked catenanes can be difficult to interpret unless the topology of the forms is known. We limited the scope of this study to the structure of torus catenanes, which are products or intermediates of DNA replication and site-specific recombination. By studying purified, individual catenane species obtained from in vitro Int recombination reactions, we were able to determine the contour of individual catenane rings in the electron micrographs. After identifying the contours of individual rings in these catenanes, we quantitated a number of properties of these molecules as functions of the number of catenane interlinks. The properties included the number of duplex DNA crossings, the distributions of pair distances between DNA segments on a single ring and on separate rings, and the center-of-mass separation between rings.

Over the range of Ca studied ($Ca \leq 18$), the structure of nicked catenanes obtained from electron micrographs lacked a regular geometry such as that shown in Fig. 1 *A*. The linkage of the highest Ca catenanes studied here is comparable only to that of a closed circular DNA containing relatively low amounts of supercoiling. The linking-number density in catenanes can be compared with that in supercoiled DNA through the ratio $\sigma_{Ca} = Ca/(2Lk_0,)$ where Lk_0 is equal to the number of DNA base pairs in the catenane divided by the DNA helical repeat (Vologodskii and Cozzarelli, 1993). Assuming a helical repeat of 10.5 bp, a catenated 3.5 kb dimer with $Ca = 18$ has a σ_{Ca} value of 0.013. Clearly, the $Ca = 18$ catenanes bear little resemblance to supercoiled molecules (Fig. 3 *D*). Recent Monte Carlo simulations of open-circular, dimeric catenanes indicate that molecules containing similar levels of linkage also appear quite irregular in geometry (Vologodskii and Cozzarelli, 1993).

Even though a regular geometry is not apparent in these catenanes, the individual rings have significant Wr. Wasserman et al. (1988) found that the right-handed wrapping of DNA in torus catenanes made by Int recombination induces a change in DNA linking number, Lk, on

religation of the DNA. The results of Monte Carlo simulations show that this result is due to induction of positive writhe by catenation (Vologodskii and Cozzarelli, 1993). The change in *Lk* was proportional to *Ca*, and with symmetric 3.5 kb catenanes identical to those studied here, approximately three catenane interlinks were required to give a unit change in either measured *Lk* or *Wr*. The ratio $Wr/\Delta Lk$ in supercoiled DNA is nearly independent of ΔLk and equal to 0.8 (Boles et al., 1990; Vologodskii et al., 1992). This difference in the amount of *Wr* induced by topological stress between supercoiled and catenated molecules may underlie the differences in geometric regularity of the two forms.

The constraint of catenation has negligible effects on the number of catenane crossings in excess of those imposed by intertwining (Fig. 4). This result implies that the structure of individual catenane rings is not strongly dependent on *Ca* when *Ca* is relatively small. Distributions of intraannular pair distances as a function of *Ca*, $P_{tra}(\rho)$, corroborate this view. We compared the distributions obtained from electron micrographs with that calculated using a simple, random-coil polymer model for the DNA rings. Remarkably, the distributions are close to those expected for planar projections of a cyclic random coil. Slight departures from the random coil model occur at $Ca = 18$, which is the upper limit of our range, and then only at large radial distances. The conclusion is that catenation has a modest effect on the extensibility of a ring because extended conformations in one ring require concurrent extension of the second ring, which is entropically unfavorable.

The distribution of pair distances between segments located on different rings, $P_{ter}(\rho)$, is quite sensitive to the value of *Ca* (Fig. 7). The radial distances corresponding to the maxima in these distributions decrease monotonically with increasing *Ca*, indicating that, on average, the rings are found progressively closer in space with increasing *Ca*. This tendency is also exhibited in the *Ca* dependence of the center-of-mass separation between rings (Fig. 7). The model for catenane structure in Fig. 1 *A*, in which the rings uniformly wind around the axis of a torus, demands that the centers of mass of the individual rings be coincident. Instead, the average center-of-mass separation at $Ca = 6$, 120 nm, is ~67% of the average radius of a single ring, 180 nm, suggesting that there are many degrees of freedom in low-complexity catenanes. Even at high *Ca* values ($Ca = 18$), the average center-of-mass separation, 30 nm, is large compared with values for the effective physical diameter of duplex DNA (Rybenkov et al., 1993; Shaw and Wang, 1993). Therefore, the Fig. 1 *A* geometry is not achieved at any value of *Ca* in the range studied here.

The strong preference for the location of interlinks in the terminal loops of singly linked supercoiled catenanes is plausibly explained in terms of the greater conformational entropy and reduced electrostatic free energy available to such conformations. Very few of these conformations had evidence of adventitious overlap between the supercoiled circles. This may be due to the high electrostatic free energy concomitant with the high charge density of tightly wound, plectonemically supercoiled conformations.

Nicked, multiply linked catenanes clearly lack resemblance to any regular geometrical model. Despite this fact, a number of quantitative and qualitative statements can be made about their structure. The relatively close agreement of the intraannular distance distribution with that of free circles suggests that individual catenane rings have considerable conformational freedom. However, the constraints imposed by increasing *Ca* lead to some coalescence of the rings. Thus, the average conformation of the catenane is determined by the balance between the elastic energy of DNA winding, the entropy of ring conformations, and the free energy of electrostatic interactions.

APPENDIX

The following derivation for the projected 2D distribution of through-space distances for 3D, cyclic random coils closely follows that of Lang et al. (1967) for linear chains. Consider the Gaussian distribution of segment distances $W(R_{i,j})$, in a cyclic, random-flights chain (Zimm and Stockmayer, 1948).

$$W(R_{i,j})dR_{i,j} = \left[\frac{3}{2\pi\mu(i,j)b^2}\right]^{3/2} \exp\left[\frac{-3R_{i,j}^2}{2\mu(i,j)b^2}\right] 4\pi R_{i,j}^2 dR_{i,j} \quad (1)$$

where $R_{i,j}$ is the through-space distance between segments i and j; b is the length of a random-flights segment; and $\mu(i,j)$ is a factor that depends on i, j, and the total number of segments in the chain N

$$\mu(i,j) = |i-j|(1 - |i-j|/N)$$

We consider here the particular case where the ith and jth segments are separated by one-half the DNA contour length. Thus $i - j = N/2$ and $\mu(i,j) = N/4$. With this simplification, Eq. 1 becomes

$$W(R)dR = \left[\frac{6}{\pi Nb^2}\right]^{3/2} \exp\left[\frac{-6R^2}{Nb^2}\right] 4\pi R^2 dR \quad (2)$$

where R is now the through-space distance from the proximal end of segment i to the distal end of segment j.

We now derive the distribution of chain segment distances for the case of a random, 2D projection of the 3D chain conformation. This is most easily done by transforming the distribution from spherical polar coordinates $\{R, \theta, \phi\}$ to cylindrical coordinates $\{\rho, \psi, z\}$. In cylindrical coordinates Eq. 2 becomes

$$W'(\rho, z)d\rho dz = \left[\frac{6}{\pi Nb^2}\right]^{3/2} \exp\left[\frac{-6(\rho^2 + z^2)}{Nb^2}\right] 2\pi\rho d\rho dz \quad (3)$$

The projected distance distribution in the ρ, ψ plane, $C(\rho)$, is easily obtained by integrating Eq. 3 over all possible values of the z coordinate.

For sufficiently long chains, the limits on this integration can be taken to be $\pm\infty$, and therefore the distance distribution becomes

$$C(\rho)d\rho = \left[\frac{12}{Nb^2}\right]\exp\left[\frac{-6\rho^2}{Nb^2}\right]\rho d\rho \qquad (4)$$

where we have used the fact that

$$\int_{-\infty}^{\infty} \exp\left[\frac{-6z^2}{Nb^2}\right]dz = \left(\frac{\pi Nb^2}{6}\right)^{1/2}$$

We thank J. Armitage for assistance with analyzing the singly linked, supercoiled catenane data and E. P. Gogol for the use of diode-array camera digitizing facilities. We also thank J. Armitage, E. P. Gogol, K. Huffman, D. Lang, and A. Vologodskii for critical comments on the manuscript.

This work was supported by National Institutes of Health grant GM31657 to N. R. C. and National Institutes of Health grant GM47898 to S. D. L. Partial support was also provided by the Permanent University Fund of the University of Texas (S. D. L.).

REFERENCES

Adams, D. E., E. M. Shekhtman, E. L. Zechiedrich, M. B. Schmid, and N. R. Cozzarelli. 1992. The role of topoisomerase IV in partitioning bacterial replicons and the structure of catenated intermediates in DNA replication. *Cell.* 71:277–288.

Barzilai, R. 1973. SV40 DNA: quantitative conversion of closed circular to open circular form by an ethidium bromide-restricted endonuclease. *J. Mol. Biol.* 74:739–742.

Benjamin, H. W., and N. R. Cozzarelli. 1986. DNA-directed synapsis in recombination: slithering and random collision of sites. *In* Proceedings of The Robert A. Welch Foundation Conferences on Chemical Research, Vol. XXIX, Genetic Chemistry: The Molecular Basis of Heredity. Robert A. Welch Foundation, Houston, TX. 107–126.

Benjamin, H. W., and N. R. Cozzarelli. 1990. Geometric arrangements of Tn3 resolvase sites. *J. Biol. Chem.* 265:6441–6447.

Bliska, J. B., and N. R. Cozzarelli. 1987. Use of site-specific recombination as a probe of DNA structure and metabolism in vivo. *J. Mol. Biol.* 194:205–218.

Boles, T. C., J. H. White, and N. R. Cozzarelli. 1990. The structure of plectonemically supercoiled DNA. *J. Mol. Biol.* 213:931–951.

Dynan, W. S., J. J. Jendrisak, D. A. Hager, and R. R. Burgess. 1981. Purification and characterization of wheat germ DNA topoisomerase I (nicking-closing enzyme). *J. Biol. Chem.* 256:5860–5865.

Frontali, C., E. Dore, A. Ferrauto, E. Gratton, A. Bettini, M. R. Pozzan, and E. Valdevit. 1979. An absolute method for the determination of the persistence length of native DNA from electron micrographs. *Biopolymers.* 18:1353–1373.

Krasnow, M. A., and N. R. Cozzarelli. 1983. Site-specific relaxation and recombination by the Tn3 resolvase: recognition of the DNA path between oriented *res* sites. *Cell.* 32:1313–1324.

Lang, D., H. Bujard, B. Wolff, and D. Russell. 1967. Electron microscopy of size and shape of viral DNA in solutions of different ionic strengths. *J. Mol. Biol.* 23:163–181.

Mizuuchi, K., M. Gellert, R. A. Weisberg, and H. A. Nash. 1980. Catenation and supercoiling in the products of bacteriophage λ integrative recombination in vitro. *J. Mol. Biol.* 141:485–494.

Nash, H. A., and C. A. Robertson. 1981. Purification and properties of the *Escherichia coli* protein factor required for λ integrative recombination. *J. Biol. Chem.* 256:9246–9253.

Nash, H. A., C. A. Robertson, E. Flamm, R. A. Weisberg, and H. I. Miller. 1987. Overproduction of *Escherichia coli* integration host factor, a protein with nonidentical subunits. *J. Bacteriol.* 169:4124–4127.

Pollock, T. J., and H. A. Nash. 1983. Knotting of DNA caused by a genetic rearrangement. Evidence for a nucleosome-like structure in site-specific recombination of bacteriophage λ. *J. Mol. Biol.* 170:1–18.

Ryan, K. A., T. A. Shapiro, C. A. Rauch, and P. T. Englund. 1988. The replication of kinetoplast DNA in trypanosomes. *Annu. Rev. Microbiol.* 42:339–358.

Rybenkov, V. V., N. R. Cozzarelli, and A. V. Vologodskii. 1993. Probability of DNA knotting and the effective diameter of the DNA double helix. *Proc. Natl. Acad. Sci. USA.* 90:5307–5311.

Sambrook, J., E. F. Fritsch, and T. Maniatis. 1989. Molecular Cloning: A Laboratory Manual, 2nd ed, Vol. 1. Cold Spring Harbor Laboratory Press, Plainview, NY. 1.21–1.53.

Shaw, S., and J. C. Wang. 1993. Knotting of a DNA chain during ring closure. *Science.* 260:533–536.

Shore, D., and R. L. Baldwin. 1983. Energetics of DNA twisting. I. Relation to twist and cyclization probability. 170:957–981.

Simpson, L. 1987. The mitochondrial genome of kinetoplastid protozoa: genomic organization, transcription, replication, and evolution. *Annu. Rev. Microbiol.* 41:363–382.

Spengler, S. J., A. Stasiak, and N. R. Cozzarelli. 1985. The stereostructure of knots and catenanes produced by phage λ integrative recombination: implications for mechanism and DNA structure. *Cell.* 42:325–334.

Sundin, O., and A. Varshavsky. 1981. Arrest of segregation leads to accumulation of highly intertwined catenated dimers: dissection of the final stages of SV40 DNA replication. *Cell.* 25:659–669.

Ullsperger, C. J., A. V. Vologodskii, and N. R. Cozzarelli. 1995. Unlinking of DNA by topoisomerases during DNA replication. *Nucleic Acids Mol. Biol.* In press.

Vologodskii, A. V., S. D. Levene, K. V. Klenin, M. D. Frank-Kamenetskii, and N. R. Cozzarelli. 1992. Conformational and thermodynamic properties of supercoiled DNA. *J. Mol. Biol.* 227:1224–1244.

Vologodskii, A. V., and N. R. Cozzarelli. 1993. Monte Carlo analysis of the structure of DNA catenanes. *J. Mol. Biol.* 232:1130–1140.

Wasserman, S. A., and N. R. Cozzarelli. 1986. Biochemical topology: applications to DNA recombination and replication. *Science.* 232: 951–960.

Wasserman, S. A., J. H. White, and N. R. Cozzarelli. 1988. The helical repeat of double-stranded DNA varies as a function of catenation and supercoiling. *Nature.* 334: 448–450.

Yamakawa, H. 1971. Modern Theory of Polymer Solutions. Harper and Row. New York, NY. 5–66.

Zimm, B. H., and W. H. Stockmayer. 1948. The dimensions of chain molecules containing branches and rings. *J. Chem. Phys.* 17:1301–1314.